Chem Soc Rev

RSC Publishing

REVIEW ARTICLE

View Article Online
View Journal

Cite this: DOI: 10.1039/c3cs60195a

How to switch a fluorophore: from undesired blinking to controlled photoswitching

Sebastian van de Linde* and Markus Sauer*

Received 11th June 2013

DOI: 10.1039/c3cs60195a

www.rsc.org/csr

Molecular optical photoswitches based on fluorescent proteins and organic dyes are fundamental for super-resolution fluorescence imaging and tracking methods. Precise control of switching, bio-labeling compatibility, and high brightness make photoswitches broadly applicable. This review emphasizes the design and development of photoswitches and the requirements they need to fulfill for their successful application in single-molecule localization microscopy. Furthermore, we discuss recent developments in improving the photoswitching performance with a special focus on organic dyes.

Introduction

The application of fluorescent probes to light microscopy advanced the technique to one of the most sensitive and versatile tools in biological research.[1] Fluorophores were either discovered in nature and transferred into science (fluorescent proteins) or synthesized (organic dyes and semiconductor nanocrystals). By tagging fluorophores specifically to proteins of interest it became possible to observe the inner life of cells and organisms at high contrast with a lateral and axial resolution of typically 200–300 nm and 500–700 nm, respectively. At the end of the 20th and the beginning of the 21st century, a new aspect of fluorophore properties attracted attention: the ability to control fluorescence emission through irradiation with light of appropriate wavelength, a phenomenon known as photoswitching. Optical switches were originally considered for optical data storage,[2] but they have also found diverse applications in fluorescence microscopy, *e.g.*, as optical highlighters.[3]

Photoswitches are molecules that can be switched between two distinct states by external means. We can assign the term photoswitch to any fluorophore that exhibits a reversible or irreversible transition from a nonfluorescent to a fluorescent state. Today a huge variety of photoswitches for fluorescence microscopy is available; the most important representatives are (i) photoswitchable FRET (fluorescence resonance energy transfer) systems, in which the fluorescence of a conventional fluorophore is selectively quenched by a switchable photochromic compound, *e.g.*, diarylethenes and spiropyrans,[4] (ii) nonfluorescent fluorophores that are irreversibly activated to a fluorescent state[3] or fluorophores that are photoconverted to a red-shifted fluorescent state,[5] and (iii) fluorophores that are reversibly switched between a fluorescent and nonfluorescent state[6–8] (Fig. 1).

Each category can be divided into subgroups, *e.g.*, the type of fluorophore (fluorescent protein or organic dye), activation and

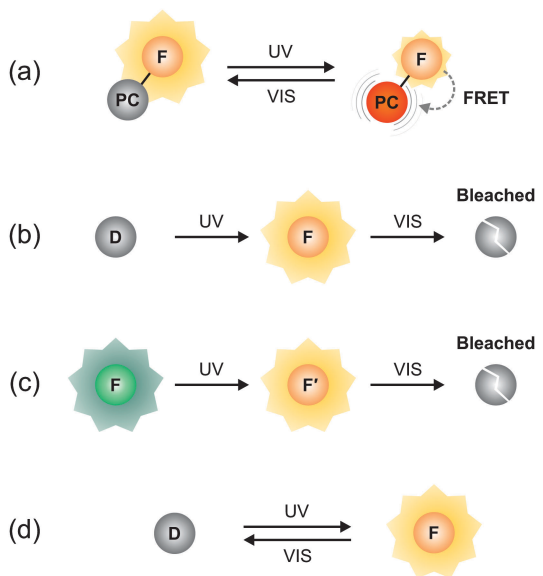

Fig. 1 Type of photoswitches. (a) Photoswitchable FRET system; upon illumination with UV light the fluorophore (F) is quenched by the photochromic compound (PC). (b) Photoactivation from a nonfluorescent *dark* (D) to a fluorescent (F) state. (c) Photoconversion from a fluorescent (F) to a red-shifted fluorescent state (F′) with photobleaching as the final step (b and c). (d) Fluorophores which are reversibly switched between a fluorescent (F) and nonfluorescent (D) state. Whereas the read-out wavelength is in the visible spectral range (VIS), activation mostly occurs at 400 nm or at shorter wavelengths (UV). The reader should note that photobleaching can also take place in schemes (a) and (d), but was left out to focus the attention on the transitions important for super-resolution imaging.

Department of Biotechnology & Biophysics, Biocenter, Julius-Maximilians-University Würzburg, Am Hubland, 97074 Würzburg, Germany.
E-mail: vdlinde@uni-wuerzburg.de, m.sauer@uni-wuerzburg.de;
Fax: +49 931 31-84509; Tel: +49 931 31-80935, +49 931 31-84507

readout wavelengths, or special buffer conditions, and will be described in more detail in the following chapters. The reason why photoswitches are widely applied in super-resolution fluorescence microscopy is the advancement of single-molecule spectroscopy since the end of the 20th century. Fluorescence intermittencies, such as singlet–triplet transitions (so-called *blinking*) within the emission pattern of single molecules, were observed for many fluorophores as a consequence of the observation of a single quantum system.[9,10] Furthermore, it became obvious that single molecules can be localized with high precision by fitting a model to their point-spread-function (PSF), whereas the precision is mainly determined by the number of collected photons and the signal-to-noise ratio.[11–13]

Both findings, separation of fluorescence emission in time and single-molecule localization, ultimately paved the way for single-molecule based super-resolution imaging and have been used advantageously for the first time to resolve blinking semiconductor nanocrystals.[14] Upon irradiation, nanocrystals typically show fluorescence intermittencies since radiative electron–hole recombination competes with non-radiative relaxation pathways. The blinking is power-law distributed and thus occurs on all time scales. Since a high-resolution image consists of many individually localized points it has been termed *pointillism*. Unfortunately, the short-lived non-fluorescent states of nanocrystals render the resolution of complex, densely labeled structures more complicated. The breakthrough was finally achieved by combining photoswitches exhibiting long-lasting dark states with precise single-molecule localization, a technique best described by the term *localization microscopy*.[15–17] In localization microscopy, photoswitches are used to label a structure of interest, *e.g.*, cellular proteins. While the majority of photoswitches are nonfluorescent, tiny subsets are stochastically activated and precisely localized over time. At any time the density of activated fluorophores must be low enough to allow single-molecule localization. Finally, an image with superior resolution is reconstructed from all localizations.

Photoactivated localization microscopy (PALM)[15] and fluorescence photoactivation localization microscopy (FPALM)[17] use photoactivatable fluorescent proteins. Stochastic optical reconstruction microscopy (STORM),[16] on the other hand, originally utilized a pair of organic dyes (Cy5–Cy3) under thiol-containing and oxygen depleted buffer conditions as a reversible switching unit.[8] The latter method was later simplified in *direct* STORM (*d*STORM),[18] which advantageously used single-dye switching (*e.g.*, Cy5 or Alexa Fluor 647), *i.e.*, in the absence of an activator fluorophore.[7] Thus, commercially available fluorescent probes could be used directly for single-molecule localization microscopy. Besides (F)PALM and (*d*)STORM, the principle of single-molecule localization was used in several variants of localization microscopy such as blink microscopy,[19] ground state depletion microscopy followed by individual molecule return,[20] or binding based approaches (see chapter 5).[21–24] During the last years, localization microscopy underwent various advancements[25–29] and has found its place among established fluorescence super-resolution imaging methods such as structured illumination microscopy (SIM)[30] and stimulated emission depletion (STED).[31]

The aim of this review is to introduce the reader to the fundamentals of photoswitches, their control by external means, and their impact on super-resolution imaging by single-molecule localization microscopy.

1 Photoswitches: definitions

In this review, we define the general term *photoswitches* as fluorophores with a reversible or irreversible transition from a nonfluorescent to a fluorescent state. At this point, it is important to stress this definition and to introduce more accurate terms. We distinguish fluorophores that are

(1) irreversibly photoactivated from a nonfluorescent (*dark*, D) state to a fluorescent state (F), termed *photoactivatable fluorophores*: $D \rightarrow F$,

(2) irreversibly photoconverted from a fluorescent state (F) to a red-shifted fluorescent state (F′), termed *photoconvertible fluorophores*: $F \rightarrow F'$, or

(3) reversibly switched between a fluorescent *on*- and non-fluorescent *off*-state, termed *photoswitchable fluorophores*: $D \rightleftharpoons F$.

In the course of this review, we do not differentiate between photoconvertible and photoactivatable fluorophores for convenience, the term photoactivatable (PA) is used for both types and we will use the following short cuts:

(1) PA-fluorophore:
- PA-FP: photoactivatable/photoconvertible fluorescent protein
- PA-dye: photoactivatable organic dye

(2) PS-fluorophore:
- PS-FP: photoswitchable fluorescent protein
- PS-dye: photoswitchable organic dye

2 Theoretical description of photoswitches

In the following we consider the reaction schemes of irreversibly photoactivatable and reversibly photoswitchable fluorophores and formulate basic rate equations to describe their temporal behavior using a general kinetic model. For further reading we would like to refer the interested reader to literature.[32]

2.1 Photoactivatable and photoconvertible fluorophores

A PA-fluorophore can be activated from the dark state D to the fluorescent state F with rate k_a. Once activated, the fluorophore is excited, read-out and photobleached (P). This photobleaching step described by rate k_p is a central element in localization microscopy methods like PALM. Activation and photobleaching are mostly considered to be irreversible processes according to the scheme

$$D \xrightarrow{k_a} F \xrightarrow{k_p} P$$

and for considering the temporal behavior of the number of molecules of each state, *i.e.*, $N_D(t)$, $N_F(t)$, $N_P(t)$, we can formulate the following rate equations:

$$\frac{dN_D(t)}{dt} = -k_a N_D(t) \quad (1)$$

$$\frac{dN_F(t)}{dt} = k_a N_D(t) - k_p N_F(t) \quad (2)$$

$$\frac{dN_P(t)}{dt} = k_p N_F(t) \quad (3)$$

Because at the beginning of the experiment all fluorophores are ideally dark, $N_D(t_0) = N_{D0}$, eqn (1) can be solved to

$$N_D(t) = N_{D0}\, e^{-k_a t}, \quad (4)$$

resulting in a monoexponential decay of dark fluorophores over time. With eqn (4) we can solve differential eqn (2) for $k_a \neq k_p$ and $N_F(t_0) = 0$:

$$N_F(t) = \frac{N_{D0} k_a}{k_p - k_a}\left(e^{-k_a t} - e^{-k_p t}\right). \quad (5)$$

Since the total number of fluorophores is $N_{D0} = N_D(t) + N_F(t) + N_P(t)$ we can solve eqn (3) for $k_a \neq k_p$, yielding

$$N_P(t) = N_{D0} + \frac{N_{D0}}{k_a - k_p}\left(k_p e^{-k_a t} - k_a e^{-k_p t}\right). \quad (6)$$

In Fig. 2 the temporal courses of the three states for constant rates are shown. The localization microscopy experiment ends as soon as every fluorophore is read-out and no fluorophore is activated anymore. Therefore, k_a and N_{D0} ultimately determine the time required to perform a localization microscopy experiment. Because at time $t_{max} = \frac{\ln(k_a/k_p)}{k_a - k_p}$ the maximum number of active fluorophores ($N_F(t_{max}) = N_{Fmax}$) is reached with

$$N_{Fmax} = N_{D0}\left(\frac{k_a}{k_p}\right)^{\frac{k_p}{k_p - k_a}} \quad (7)$$

(*cf.* Fig. 2(b)), it is often desirable to adjust k_a during the experiment to keep the number of active fluorophores constant thus reducing the total acquisition time, *e.g.*, by increasing the irradiation intensity of the activation laser.

Steady-state approximation. In localization microscopy experiments, k_a is usually very low in order to activate only small fractions of fluorescent molecules. On the other hand, k_p must be high enough to bleach activated fluorophores quickly, which then creates 'dark space' for subsequent activated emitters. For $k_p \gg k_a$, every photoactivated fluorophore is photobleached quickly, and we can consider the temporal change of active emitters to be constant, *i.e.*, $dN_F/dt = 0$ (Bodenstein approximation[33]). Then, the active emitter density is controlled by the ratio of both rates as eqn (2) results in

$$N_F(t) = N_D(t)\frac{k_a}{k_p}. \quad (8)$$

In addition, eqn (3) can be rewritten as $dN_P/dt = k_a N_D$ and (using eqn (4)) solved to

$$N_P(t) = N_{D0}(1 - e^{-k_a t}). \quad (9)$$

For the steady-state approximation, $N_D(t)$, $N_F(t)$, and $N_P(t)$ can be described by eqn (4), (8), and (9) (Fig. 2(b)).

The rate k_p and therefore the fluorophore's average dwell time in the fluorescent state is mainly controlled by the readout

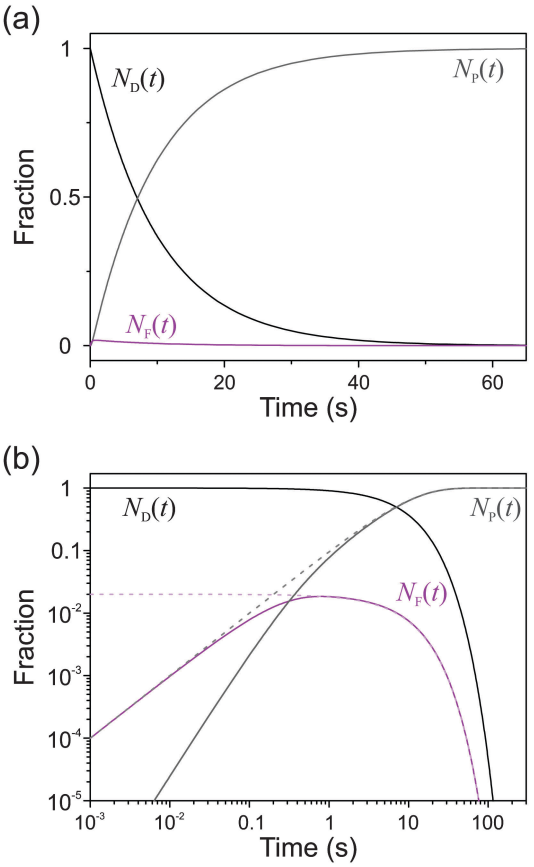

Fig. 2 Time course of a PA-fluorophore population showing the fraction of fluorophores in the dark (black), fluorescent (magenta), and photobleached state (gray) with activation rate $k_a = 0.1\ s^{-1}$ and photobleaching rate $k_p = 5\ s^{-1}$; $t_{max} = 0.8$ s and $N_{Fmax} = 1.85\%$. (a) The linear and (b) log–log plot of the underlying kinetics according to eqn (4)–(6). Light magenta ($N_F(t)$) and light gray ($N_P(t)$) dashed lines in (b) represent the steady-state approximation.

wavelength intensity I_{ex} (*e.g.*, 488 nm). In real experiments, one has to consider that the fluorophore's dark state is not only excited by the activation light intensity I_{ac} (*e.g.*, at 405 nm) but also, albeit inefficiently, by the readout wavelength. Therefore, k_a is a function of I_{ac} and I_{ex}. If I_{ex} is high enough, the density of activated molecules can be temporarily sufficient for localization microscopy even if no additional laser for activation is used.

2.2 Photoswitchable fluorophores

Photoswitchable fluorophores are switched reversibly between a fluorescent *on*- (F) and nonfluorescent *off*-state (D) with rates k_{off} and k_{on}, respectively, according to the scheme

$$F \underset{k_{on}}{\overset{k_{off}}{\rightleftharpoons}} D.$$

For convenience, we do not consider possible photobleaching pathways in this scheme. Therefore, we use the following rate equations for the temporal behavior of the number of molecules of each state ($N_D(t)$ and $N_F(t)$):

$$\frac{dN_F(t)}{dt} = -k_{off} N_F + k_{on} N_D \quad (10)$$

$$\frac{dN_D(t)}{dt} = k_{off}N_F - k_{on}N_D \quad (11)$$

Usually, at the beginning of a localization microscopy experiment all photoswitchable fluorophores reside in their fluorescent *on*-state. With $N_F(t_0) = N_{F0}$ and $N_{F0} = N_F(t) + N_D(t)$ we can solve eqn (10) to

$$N_F(t) = N_{F0}\left(\frac{k_{on}}{k_{off}+k_{on}} + \frac{k_{off}}{k_{off}+k_{on}}e^{-(k_{off}+k_{on})t}\right). \quad (12)$$

Considering $N_D(t_0) = 0$, the solution of eqn (11) is

$$N_D(t) = \frac{N_{F0}k_{off}}{k_{off}+k_{on}}\left(1 - e^{-(k_{off}+k_{on})t}\right). \quad (13)$$

With proceeding time ($t \rightarrow \infty$) equilibrium is reached

$$N_{D_{eq}} = \lim_{t\to\infty} N_D(t) = \frac{N_{F0}k_{off}}{k_{off}+k_{on}} \quad (14)$$

$$N_{F_{eq}} = \lim_{t\to\infty} N_F(t) = \frac{N_{F0}k_{on}}{k_{off}+k_{on}} \quad (15)$$

i.e., $dN_F/dt = 0$ and $dN_D/dt = 0$, meaning that a constant fraction of fluorescent and nonfluorescent fluorophores is maintained ($N_{D_{eq}}$ and $N_{F_{eq}}$). Rearrangement of eqn (14) and (15) leads to

$$\frac{N_{D_{eq}}}{N_{F_{eq}}} = \frac{k_{off}}{k_{on}}. \quad (16)$$

The switching rates control the fluorophore's average dwell time in the *on*- and *off*-state with $\tau_{on} = k_{off}^{-1}$ and $\tau_{off} = k_{on}^{-1}$. Therefore the ratio $k_{off}/k_{on} = \tau_{off}/\tau_{on}$ is directly linked to the active emitter density. In Fig. 3 the time course of an experiment with photoswitchable dyes is exemplified. With $k_{off}/k_{on} = 300$, at equilibrium 0.33% of all fluorophores reside in their fluorescent state at any time. This ratio is of fundamental importance for localization microscopy with PS-fluorophores, since it determines the number of active fluorescent molecules per area. When the density of fluorophores is too high or switching rates are set inappropriately, more than one fluorophore can be fluorescent per diffraction-limited area with the result of false-positive localizations and image artifacts (see chapter 3).

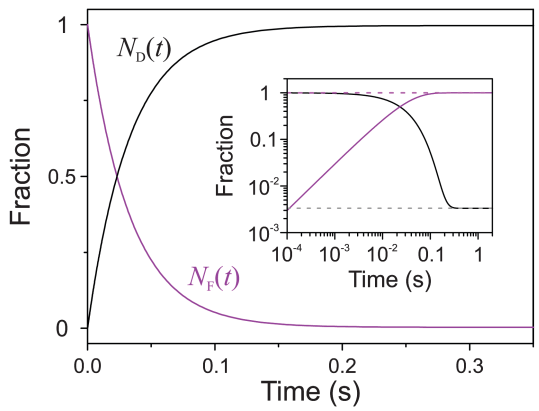

Fig. 3 Time course of a PS-fluorophore population showing the fraction of fluorophores in the dark (black) and fluorescent (magenta) state with $k_{off} = 30\ s^{-1}$ and $k_{on} = 0.1\ s^{-1}$. A linear plot of the underlying kinetics according to eqn (12) and (13), inset: log–log plot. Light magenta and gray dashed lines represent the equilibrium fraction of the fluorescent and dark state, respectively; $N_{F_{eq}} = 0.33\%$.

Experimentally, switching rates can be influenced by several external means. For example, the carbocyanine dye Cy5 can be switched *off* through irradiation at 640 nm and *on* through irradiation at shorter wavelengths, *e.g.*, 400–500 nm in the presence of thiols.[7,8] The switching rates k_{on} and k_{off} scale linearly with the applied laser power,[18,34] but strong irradiation with only the read-out wavelength at 640 nm switches also a certain fraction of molecules to the *on*-state, a behavior similar to PA-fluorophores. Other means to control the photoswitching rates of PS-dyes include application of different switching buffer compositions (see Chapter 4.1).

3 Localization of single-molecules and reconstruction of super-resolution images

Localization microscopy uses wide-field fluorescence microscopy schemes and sensitive cameras, *e.g.*, charge-coupled devices (CCD), for single-molecule detection. Due to the wave-nature of light, every single fluorophore is imaged as a blurred spot, *i.e.*, the photons are distributed according to the point-spread-function (PSF) of the microscope in the imaging plane. However, the position of single, isolated objects can be approximated, *e.g.*, by fitting a two-dimensional Gaussian function to the measured emission profile. The error of the position determination, *i.e.*, the localization precision, depends on the number of collected photons (N), the pixel size of the camera (a), the standard deviation of the PSF (σ), and the background noise (b)[12,35] and is often simplified to $\sigma/\sqrt{N}$.

According to Mortensen *et al.* (2010) the variance of the localization error $\mathrm{Var}(\mu_x)$ can be described as

$$\mathrm{Var}(\mu_x) = \frac{\sigma_a^2}{N}\left(\frac{16}{9} + \frac{8\pi\sigma_a^2 b^2}{Na^2}\right), \quad (17)$$

with $\sigma_a^2 = \sigma^2 + a^2/12$ and $a \leq \sigma$. In addition, if an electron multiplying CCD (EMCCD) camera is used, μ_x is calculated as the square root of twice the variance in order to account for the excess noise introduced by the electron multiplying process.[35] Imaging fluorophores with an EMCCD camera with $N = 1000$ photons, $a = 120$ nm, $\sigma = 135$ nm, and $b^2 = 20$ photons leads to $\mu_x \approx 10$ nm. These considerations instantly highlight the importance of techniques, *e.g.*, special buffer compositions, to increase the photon yield emitted per fluorophore and switching event. Organic dyes can easily provide several thousands of photons per *on*-state and therefore ensure better localization precisions than fluorescent proteins with several hundred of photons per *on*-state. Since a high signal-to-background ratio is crucial for single-molecule localization, wide-field microscopy with total internal reflection fluorescence (TIRF) or inclined illumination schemes[36] are widely applied.

Localization of fluorophores was first used in single-molecule tracking experiments.[11,13] For instance, the molecular motor protein Myosin V was labeled with the organic dye Cy3 and its movement along immobilized F-actin filaments was observed

with TIRF microscopy.[13] With this method, termed fluorescence imaging with one nanometer accuracy (FIONA), the center of mass of each Cy3 was localized over time and stepping traces of individual Myosin V molecules were generated revealing a hand-over-hand model of motility.[13] In order to be applicable for tracking experiments fluorophores have to exhibit a high fluorescence quantum yield (brightness) and stable fluorescence emission ideally uninterrupted by fluorescence intermittencies. Furthermore, the density of recorded fluorophores must be low enough to avoid overlapping PSFs and out-of-focus fluorescence background.

The advent of photoswitches paved the way for labeling biological structures at high densities. With the majority of labels remaining nonfluorescent, only a sparse subset of fluorescent molecules is (i) stochastically activated, (ii) read-out, and (iii) bleached or switched *off*. The cycle (i–iii) is repeated several thousands of times and an image stack is recorded with a sensitive camera (*e.g.*, CCD, EMCCD, or scientific complementary metal oxide semiconductor (sCMOS)). Next, each PSF in every frame containing a minimum freely-selectable number of photons (threshold) has to be identified, analyzed and fitted. Its coordinates are finally stored in a text file and an artificial image is reconstructed from all localizations.

The most prominent types of super-resolution image reconstruction are probability maps or histograms of all localizations. Using the probability map, each localization is convolved with a 2D Gaussian function with a width according to its corresponding localization precision, which is derived from the amount of collected photons. Alternatively, coordinates are binned and histogrammed in 2D, *e.g.*, with 10 nm sub-pixel size, where the color code represents the occurrence of localization events in every sub-pixel. Here, the type of photoswitch influences the reconstructed super-resolution image. PA-fluorophores are considered to be localized only once if all photons of the *on*-state are combined, whereas PS-fluorophores are usually switched multiple times and thus generate a localization pattern. The localization pattern has the advantage of reflecting that the fluorophore's position was probed multiple times. Its full width at half maximum (FWHM) is often referred to as the experimental localization precision.

Because in localization microscopy the super-resolved image is reconstructed from single-molecule localization events, it permits access to molecular densities and explicit numbers of molecules. Here, PA-FPs with a unique, irreversible transition to the *on*-state can be advantageously used for protein quantification, since every activation event represents a protein count. Unfortunately, some PA-FPs also show transient *off*/*on* blinking as in the case of mEOS2 or Dendra2[37,38] and can lead to re-counting of the same fluorophore. In order to extract reliable protein numbers, strategies have been developed to overcome iterated counting of FPs by exploiting the time dependence of photoswitching of individual PA-FPs.[39–41] Similarly, to extract the typical average number of localizations detected per PS-fluorophore, calibration experiments in the same cellular nanoenvironment with different concentrations of active fluorophores are indispensable.

Today, real-time computation of super-resolution images is possible[43–45] and open-source software is available, *e.g.*, rapid*d*-STORM.[46] However, the performance of single-molecule fitting algorithms is strongly influenced by the active emitter density since overlapping PSFs of adjacent fluorophores are more difficult to analyze.[42] The analysis of (overlapping) PSFs can either lead to correct localizations (true positives), incorrect localizations (false positives), or the analysis of the PSF is aborted (lost localization), *e.g.*, for reasons of asymmetry. With increasing emitter density the fraction of true positives decreases whereas the fraction of false positives increases. This can be measured by considering two algorithm characteristics, *i.e.*, *recall* and *stochastic precision* (Fig. 4).[42] The recall is defined as the number of true positive localizations divided by the number of all emitters that should have been localized and the stochastic precision as the number of true positive localizations divided by all localizations made (true and false positives).

The recall is an important parameter for PA-fluorophores because every fluorophore is probably activated only once and if emitters are not localized the information is irretrievably lost. For PS-fluorophores lost localizations can be compensated when the fluorophore is switched *on* again. Therefore, stochastic precision is the relevant factor for PS-fluorophores. Even if the recall is low for PS-fluorophores, the stochastic precision can be high enough to reconstruct a super-resolution image, *e.g.*, 30% recall and 80% stochastic precision as shown in Fig. 4(ii). For generating an image using PS-fluorophores with at least 80%

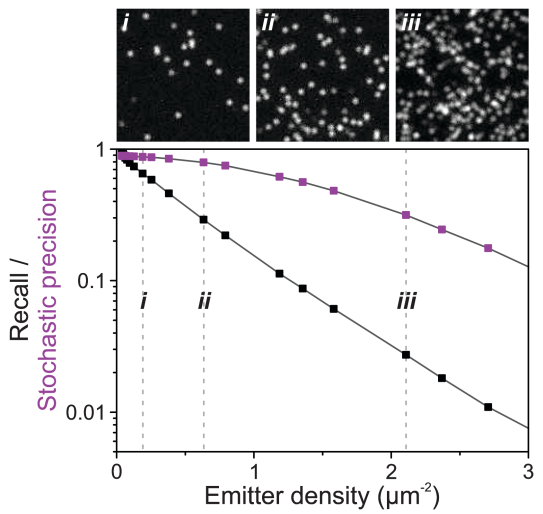

Fig. 4 Simulated data showing the localization performance of a single-molecule fitting algorithm as a function of the emitter density. Top: typical snapshots of single-molecule movies shown for different emitter densities ((i) 0.19 μm^{-2}, (ii) 0.63 μm^{-2}, (iii) 2.11 μm^{-2}). Bottom: recall (black), *i.e.*, the percentage of correct (true positive) localizations to all emitters that should have been localized, and stochastic precision (magenta), *i.e.*, the percentage of true positive localizations to all localizations made (true and false positives) as a function of the emitter density (default simulation parameters:[42] simulated fluorophores spaced on a 40 nm lattice, 0.1 s camera integration time, τ_{on} = 0.3 s, 10 kHz photon count rate, multi-emitter search, τ_{off} was varied for different emitter densities; for full information we refer the reader to ref. 42). Analysis was performed with rapid*d*STORM.

stochastic precision, the emitter density for classical single-molecule fitting algorithms should not exceed 0.6 emitter μm^{-2} (Fig. 4, magenta curve). The requirements for PA-fluorophores are even more challenging; a recall of better than 60% can only be achieved with <0.2 emitter μm^{-2} (Fig. 4, black curve) using the default settings as described in ref. 42.

As described in the previous chapters, switching and activation rates of PS- and PA-fluorophores determine the emitter density. If the emitter density exceeds a critical threshold – either due to an increased activation rate or higher structural complexity – overlapping PSFs cannot be localized appropriately. Consequently the fluorophores true positions are lost and, if not discarded, false positive localizations are introduced, which lead to artifacts in the reconstructed super-resolution image. As shown in Fig. 5, high emitter densities lead to false positive localizations between adjacent filaments and thus the structural resolution effectively decreases. In other words, for the experimentalist the emitter density per frame is an important first estimator for the achievable quality of the reconstructed super-resolution image. Subsequent data analysis, *e.g.*, quantification and meaningful cluster analysis, can only be performed if the single-molecule data was recorded at appropriate density.

When following dynamics in living cells, a fundamental tradeoff between structural and temporal resolution must be considered.[48] Here, it is beneficial to tolerate higher emitter densities as structural features can be resolved in shorter time periods. Therefore, there is increasing demand for new reconstruction methods. First strategies have been developed that can currently handle one order of magnitude higher emitter densities compared to single-molecule fitting algorithms albeit at lower localization precision, *e.g.*, DAOSTORM[49] and compressed sensing.[50]

4 Photoswitching mechanisms of fluorophores

Both types of fluorophores, FPs and organic dyes, can be manipulated to act either as reversibly photoswitchable or irreversibly photoactivatable fluorophores. Therefore, we split this section in two chapters: organic dyes (Chapter 4.1) and FPs (Chapter 4.2).

4.1 Controlling switching performance of organic dyes

Minimizing photobleaching and suppressing blinking of organic dyes. Besides the chromophore's molecular structure, photophysics of organic dyes is also influenced by solvent and co-solutes. If we monitor the fluorescence emission of a single organic dye in aqueous solution over time, we observe an almost constant fluorescence emission until the dye is photobleached – interrupted only by short excursions to the triplet state. The fact that emission is only briefly interrupted can be explained by the high concentration of dissolved molecular oxygen from air ($\sim$250 μM). Upon irradiation, the fluorophore is mainly cycled between the singlet ground (S_0) and first excited singlet state (S_1). Dependent on its intersystem crossing probability the triplet state (T) will be populated. The triplet state of organic dyes exhibits lifetimes typically in the range of a few microseconds, *i.e.*, several orders of magnitude longer than the fluorescence lifetime of the excited singlet state of only a

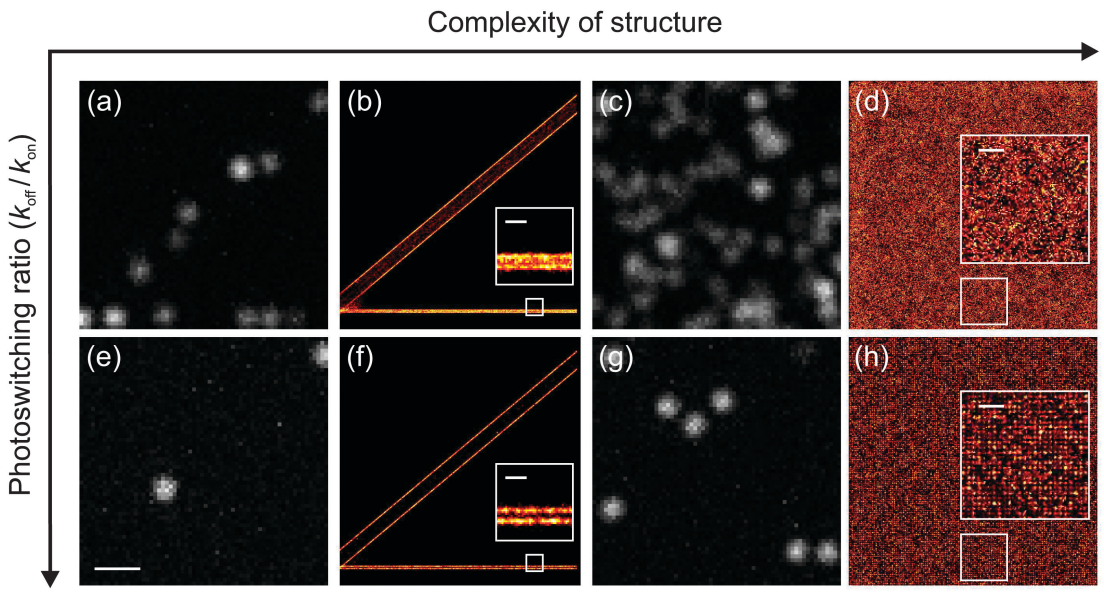

Fig. 5 Simulated data demonstrating the influence of the ratio of photoswitching rates of PS-fluorophores, k_{off}/k_{on}, on different structural complexities. With increasing complexity of the imaged structure and/or decreasing k_{off}/k_{on}, the number of emitters present per area increases generating artifacts in the reconstructed super-resolution image as a possible result. Single-molecule stack simulated with (a–d) k_{off}/k_{on} = 250 and (e–h) k_{off}/k_{on} = 3000. (a, c, e and g) Snapshots from the localization microscopy stacks from which the reconstructed super-resolution images (b, d, f and h) were generated. (b and f) Pairs of lines separated by 300 and 50 nm with a fluorophore attached every 8.5 nm. (d and h) A lattice with 40 nm fluorophore spacing. Scale bars: (e) 1 μm (valid for all images); insets in (b) and (f) 100 nm; insets in (d) and (h) 200 nm. Reproduced from ref. 47 with permission.

few nanoseconds. Thus, the triplet state is prone to collision-induced reactions with reaction partners. Since oxygen resides in a ground state triplet under standard conditions, it efficiently quenches the dye's triplet state and repopulates the S_0 state. Therefore, the triplet state is quenched resulting in short microsecond fluorescence intermittencies that are masked in single-molecule fluorescence imaging experiments with typical frame rates of 1–100 Hz. However, as a quenching product, singlet oxygen is generated – a highly reactive oxygen species (ROS) – responsible for cellular photodamage and possibly also involved in fluorophore photobleaching.

The first approach of stabilizing fluorescence emission was the removal of molecular oxygen by either purging the solution with oxygen-free gas or by enzymatic digestion. The most popular enzymatic oxygen scavenger system is a cocktail of glucose oxidase, catalase and β-D-glucose as a substrate,[51] but also protocatechuate-dioxygenase/3,4-protocatechuic acid[52] or pyranose oxidase/catalase/β-D-glucose[53] have been used. The absence of oxygen, however, increases the triplet state lifetime and thus accounts for the appearance of blinking events in single-molecule imaging experiments. Therefore, triplet quenchers and reducing agents such as β-mercaptoethanol[54] or Trolox (6-hydroxy-2,5,7,8-tetramethylchroman-2-carboxylic acid) were added in order to obtain prolonged and stable fluorescence emission.[55,56] Besides mercaptoethanol also β-mercaptoethylamine (MEA), cyclooctatetraene (COT) or potassium iodide (KI) are used as triplet quenchers.[57,58] Interestingly, it has been reported that the heavy atom effect of KI does not only promote triplet state formation but can also decrease the triplet state lifetime by a charge-coupled deactivation mechanism for some dyes absorbing in the green wavelength range.[58]

Finally, a refined system termed the reducing and oxidizing system (ROXS) was developed to stabilize fluorescence emission through a holistic view on the reaction pathways of organic dyes.[59] Using ROXS, micro- to millimolar concentrations of reducing and oxidizing agents such as ascorbic acid (AA) and methylviologen (MV) are added to an oxygen-depleted aqueous buffer. The concentration of the oxidizer and reducer has to be kept low in order to minimize collision-induced singlet-state quenching but enable selective quenching of fluorophores residing in the triplet state by either reduction or oxidation to the corresponding semi-reduced radical anion or semi-oxidized cation, respectively. Next, the produced anion or cation is oxidized or reduced again, respectively, and the singlet ground state repopulated. In summary, the fluorophore is cycled efficiently between S_0 and S_1 states with only minimal interruptions in fluorescence emission, thus minimizing photobleaching and enabling the monitoring of single-molecule trajectories for extended periods of time.

Generating long-lasting, 'stable' dark states. At first sight, stabilizing fluorescence emission seems somewhat contradictory to photoswitching. However, long-lasting *off*-states can be generated using chemical buffers, as described above, implementing slight variations in buffer composition, *e.g.*, the concentration of reducing and oxidizing agents.

The first buffer-controlled photoswitch was found through imaging the carbocyanine dye Cy5 in oxygen depleted aqueous buffer containing β-mercaptoethanol or β-mercaptoethylamine (MEA) as a triplet state quencher and reducing agent.[7,8] The fluorescence of Cy5 was monitored upon irradiation with red laser light (*e.g.*, 633 nm) until the dye entered a metastable dark state. Upon irradiation at a shorter wavelength (*e.g.*, 337, 488, 532 nm) the dye switches back to the *on*-state. In these studies, switching of Cy5 was performed directly[7] or by using a reporter–activator dye pair, *e.g.*, Cy5–Cy3.[8] In the latter case, the close proximity between the two dyes facilitates *on*-switching of the reporter (*e.g.*, Cy5) at lower laser power. Photoswitching of carbocyanine dyes has been further extended to other carbocyanine derivatives such as Alexa Fluor 647, Cy5.5, Cy7, Alexa Fluor 680, Alexa Fluor 700, and Alexa Fluor 750.[7,18,34,47,62,63]

Interestingly, it was observed that aqueous buffers containing thiols like MEA can not only serve as switching media but also as efficient oxygen scavenger systems.[64] A solution with >10 mM MEA is sufficient to deplete molecular oxygen within tens of minutes to levels that are suitable for super-resolution imaging.[61,65] Oxygen scavenging can be further accelerated with increasing thiol concentrations, changes in pH value, or with the addition of μM concentrations of methylene blue (MB). MB, an almost nonfluorescent thiazine dye with a high triplet yield, is reduced by MEA in a two-step reaction to the colorless leuco form (MBH) (similar to the scheme in Fig. 6). MBH can be oxidized back to MB by O_2. This cycle can be repeated until the sacrificial reducing agent is exhausted or O_2 is consumed.[64] Thiols therefore do not only act as triplet state quenchers of organic dyes, but also as oxygen scavengers.

Besides cyanine dyes, photoswitching can be also extended to other classes of dyes such as rhodamines and oxazines with various buffer compositions, most of them containing reducing agents. For example, photoswitching has been demonstrated in the presence of millimolar concentrations of thiols,[61,65,66] with

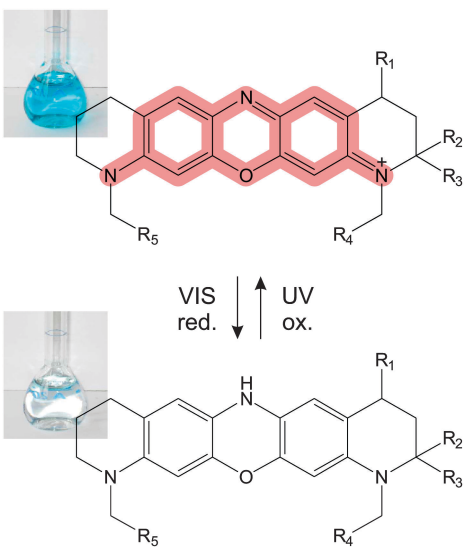

Fig. 6 Reversible photoswitching of oxazine dyes like ATTO 655 in presence of thiol-containing reducing agents such as MEA and upon irradiation at 640 nm and 405 nm, respectively. During the reaction oxygen is consumed and a stable colorless dark state is formed.[60,61]

tris(2-carboxyethyl)phosphine (TCEP),[67] and a combination of reducing and oxidizing agents.[19,55,68] As metastable dark states, semi-reduced dye radicals,[19,61,65] leuco forms[60,61] (Fig. 6), thiol[69] and phosphine adducts[67] have been proposed and identified, respectively, whereas all dark states share the common ground: a reduced chromophore with split π-electron systems. Therefore, dark state absorption is shifted to shorter wavelengths enabling reactivation of the *on*-state upon irradiation at 350–550 nm.[47,61,66]

Besides read-out and activation wavelength, important parameters to influence *on*- and *off*-switching rates include the concentration of reducing agents,[19,61,65,67,69] oxidizing agents,[68] pH value of the solution,[65] and the application of enzymatic scavenger systems.[64,66] Localization microscopy with organic dyes has also been performed successfully in living cells exploiting directly the (reducing) cellular redox environment for photoswitching[29,70] or adding thiols and oxygen scavengers to the cell medium.[71]

Another approach is the formation of stable hydrogenated fluorophores that serve as dark states. For instance, it has been described that carbocyanine dyes like Cy3, Cy5, Cy7 can be reduced efficiently with sodium borohydride ($NaBH_4$).[72] The resulting non-fluorescent hydrocyanines can be used advantageously for localization microscopy if one succeeds to oxidize only sparse subsets of hydrocyanines to the fluorescent form.[27] Furthermore, it has been proposed that hydrocyanines can potentially be used as sensors to probe the oxidation properties of cellular compartments in living cells. Here, oxidation could be directly monitored by the local increase in fluorescence intensity.[27]

Standard fluorophores can also be hydrogenated through $NaBH_4$ after immunofluorescence labeling as demonstrated for the cyanine dyes Cy3, Cy3B, Alexa Fluor 647, Cy5.5, and the rhodamine dye ATTO 488[73] (Fig. 7). Upon activation at 405 nm, the fluorescent form of the dye is recovered, which can be read-out and used for localization. The recovery fraction depends on the dye and ranges between 12% and 66%, *e.g.*, 35–40% for Cy3B. To stabilize the fluorescence of the activated form and prolong the *on*-state lifetime τ_{on}, the reducing buffer has been replaced by the ROXS buffer.[59] As a result, the acquisition time of the experiment increases due to the prolonged *on*-state lifetime, but the total photon yield increases as well and can reach up to 10^4 to 10^6 photons per *on*-state depending on the fluorophore used. This improves the localization precision to a few nanometers if drift over the course of the experiment is minimized and corrected in the analysis.[73]

The concept of photoactivation of organic fluorophores is also used by azido push–pull fluorophores[74] or photochromic dyes,[75,76] which all follow the classic PALM concept, where the fluorophores reside initially in a dark state and only a subset of fluorophores is photoactivated at any time of the experiment for fluorescence read-out until photobleaching occurs. For instance photochromic rhodamine amides can exist in a nonfluorescent closed (lactam) and a fluorescent open form.[77] Introducing 4-aminophthalimide into the carboxyphenyl ring of rhodamine B, Fölling *et al.* designed a photochromic fluorophore suitable for localization microscopy.[75] Such photochromic rhodamine dyes are photoactivated with UV light, but can spontaneously return to the closed form and thus be considered as reversible photoswitches. However, when embedded in polyvinylalkohol (PVA) the lifetime of the open form exceeds hours and the dye behaves like a PA-fluorophore.[75]

4.2 Controlling photoactivatable and photoswitchable FPs

Molecular basis of photoactivation and photoswitching. Today, a huge variety of PA- and PS-FPs across the visible wavelength range is available with diverse mechanisms responsible for photoactivation and/or photoswitching. For further information we would like to refer the reader to excellent reviews.[78,79] FPs are over

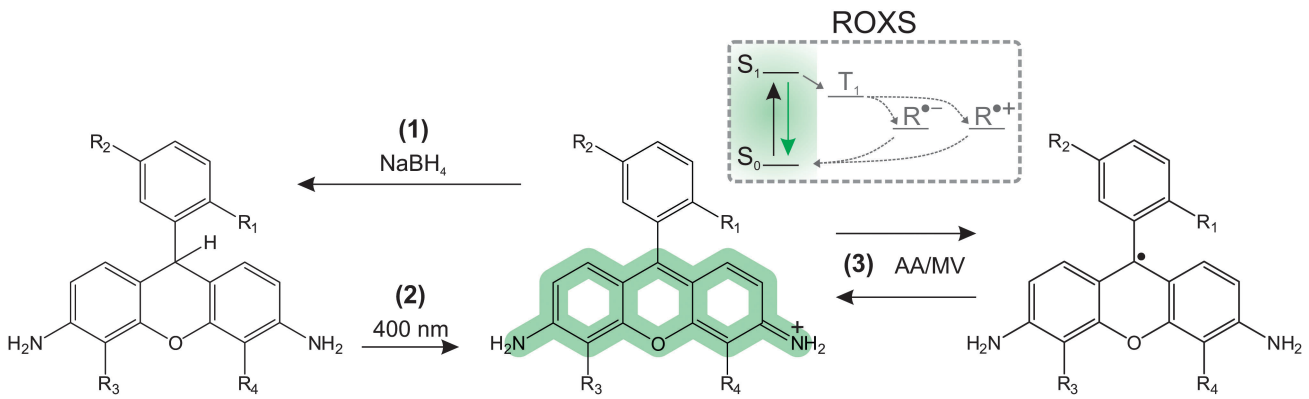

Fig. 7 Creation of PA-dyes for localization microscopy through $NaBH_4$. Conventional organic dyes (*e.g.*, ATTO 488) are hydrogenated with $NaBH_4$ to a stable fully-reduced dark state (1). $NaBH_4$ is then replaced by a ROXS buffer, which consists of ascorbic acid (AA) and methylviologen (MV) as reducing and oxidizing agents, respectively.[59] During the localization microscopy experiment, small subsets of hydrogenated dyes are activated by means of irradiation at ~400 nm (2). The fluorescence of each activated dye is read-out and stabilized by ROXS (3), *i.e.*, when entering the triplet state the dye is reduced/oxidized to a semi-reduced or semi-oxidized radical anion or cation, respectively, which is subsequently oxidized/reduced to restore the singlet ground state (S_0). The dye is then predominantly cycled between S_0 and S_1 states with minimal fluorescence intermittencies resulting in a high photon yield before photobleaching occurs. Here, it is important, that the oxidizing agent methylviologen used in ROXS does not oxidize the hydrogenated dark state (left). Activation of the dark state (2) is repeated until each dye is read-out. Right: for convenience only the semi-reduced radical is shown.

200 amino acids in length, and after proper protein folding, the inner chromophore of FPs formed out of three amino acids, *e.g.*, serine, tyrosine, and glycine for GFP, is surrounded by the so-called beta-barrel. PA-GFP is an engineered modification of wild type GFP, which was originally discovered in the jellyfish *Aequorea victoria*. In PA-GFP the substitution of threonine at position 203 (T203) with histidine (T203H) leads to a dramatic decrease in absorption around 500 nm while the peak at 400 nm is still maintained. Photoconversion of PA-GFP is induced by irradiation at 400 nm, *i.e.*, through decarboxylation of the amino acid glutamic acid at position 222 and the neutral chromophore becomes anionic.[3] Decarboxylation also takes place in wild-type GFP but with only low contrast when excited at 488 nm after photoactivation, whereas fluorescence of PA-GFP increases ~100 fold upon activation.[3]

Other PA-FPs were found in corals, *e.g.*, Kaede was isolated from *Trachyphyllia geoffroyi*[82] and EosFP from *Lobophyllia hemprichii*,[5] which are representatives of green-to-red photoconversion. The chromophore of both FPs is formed of histidine, tyrosine, and glycine. The fluorescence of the green form of Kaede and EosFP stems from the chromophore formed by the amino acids tyrosine and glycine. After photoconversion (irradiation at ~400 nm) the photochromic system is prolonged through the cleavage of a side chain of histidine[80,81] (Fig. 8), resulting in red-shifted absorption at 570 nm. Upon excitation, fluorescence can be detected until the chromophore is photobleached. The advantage of PA-FPs like EosFP over PA-GFP is that cellular structures can be observed before single-molecule photoconversion is induced, which eases preselection of the region of interest in localization microscopy experiments.

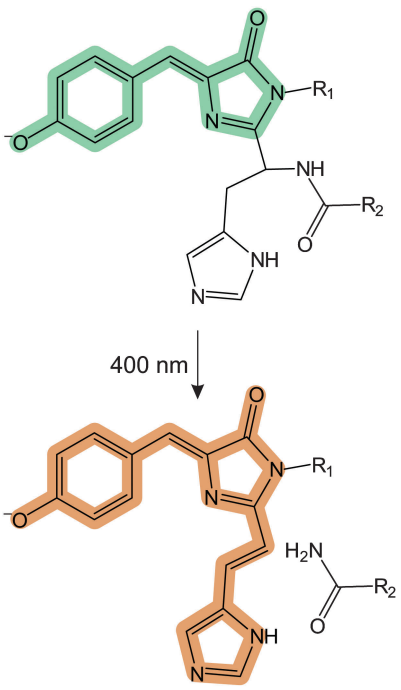

Fig. 8 Green and red-shifted chromophore systems of Kaede and EosFP. For the full proposed reaction mechanism see ref. 80 and 81. Photoinduced cleavage between His-Cα and Nα side chains extends the chromophore system with red-shifted absorption (506 → 569 nm) and fluorescence emission (516 → 581 nm).

Dronpa was cloned from Pectiniidae and shows reversible photoswitching between a fluorescent *on*- and nonfluorescent *off*-state.[6] Irradiation at 488 nm excites the fluorophore and fluorescence photons are emitted until switching to the dark state occurs. Irradiation at 405 nm can switch the fluorophore back to the *on*-state. Photoswitching of Dronpa is thought to result from the interplay of *cis–trans* isomerization and the change in protonation of the cysteine-tyrosine-glycine derived chromophore.[83]

In contrast to organic dyes, activation and switching rates of PA- and PS-FPs are mainly controlled by the irradiation wavelength. However, it was demonstrated that the PA-FP mEOS2 changes its switching performance to a PS-FP when thiol-containing reducing agents (*e.g.*, MEA) are added at millimolar concentrations to standard buffers.[84]

Recent advances in FP engineering. The ongoing success of PA-FPs such as PA-GFP[3] or EosFP[5] has initiated the developments of refined variants, *e.g.*, mEOS2,[85] Dendra2,[86] or PA-mCherry1.[87] Furthermore, a variant of EosFP termed IrisFP has been developed that combines photoswitching and photoactivation properties.[88] It has two fluorescent states – green (F) and redshifted (F′) – and an irreversible transition between both states initiated upon irradiation at 405 nm with a conversion rate k_c. However, both states can be switched reversibly between an *on*- and *off*-state according to the following scheme:

$$\mathrm{D} \underset{k_{\mathrm{off}}}{\overset{k_{\mathrm{on}}}{\rightleftharpoons}} \mathrm{F} \xrightarrow{k_c} \mathrm{F}' \underset{k_{\mathrm{on}}'}{\overset{k_{\mathrm{off}}'}{\rightleftharpoons}} \mathrm{D}'$$

One of the latest achievements in PS-FPs is a reversible switchable variant of EGFP, termed rsEGFP,[89] which has been developed for STED-like super-resolution imaging following the RESOLFT concept (standing for reversible saturable optical fluorescence transitions). Using rsEGFP super-resolution imaging with <40 nm resolution has been demonstrated in living cells with irradiation intensities of the depletion laser in the range of only 1 kW cm^{-2}, which is 6 orders of magnitude lower than in classical STED microscopy.[89]

Because all PS-fluorophores are read-out and switched *off* at the same wavelength, the photon number detected per *on*-state cannot be controlled. Especially for some PA-FPs, the photon yield is very low, thus compromising the localization precision. Besides *on*- and *off*-switching, the scheme could be extended by a third wavelength only for probing the *on*-state.[90] Recently, a new reversible photoswitchable GFP variant termed Dreiklang has been introduced that fulfills the requirements.[91] Dreiklang is excited at 515 nm and switched *off* and *on* at 405 and 365 nm, respectively. Dreiklang has been successfully used for localization microscopy as well as for RESOLFT microscopy.

5 Localization microscopy without photoswitches

In the previous chapters we discussed photoswitches, which can be used for localization microscopy on the basis of long-lasting dark states, either created through buffer additives

(organic dyes) or bioengineering (FPs). However, there are also other localization microscopy concepts that do not use photoswitches. Examples include points accumulation for imaging in nanoscale topography (PAINT),[21] universal PAINT (uPAINT),[23] nanometer accuracy by stochastic catalytic reactions (NASCA) microscopy,[22] and binding-activated localization microscopy (BALM).[24] These concepts rely on localization of fluorescent probes or reactants that are transiently bound to or – in case of nonfluorescent substrates – activated by the structure of interest. In the case of transient binding, fluorescent probes are added to a sample, which is permanently irradiated by the readout laser. During diffusion, stochastic binding on the structure occurs followed by dissociation and/or photobleaching. The probe concentrations controls the *binding rate*, *i.e.*, the number of binding events per time.

In PAINT, binding events of fluorescent molecules on surfaces, *e.g.*, cellular membranes are detected. NASCA uses fluorogenic compounds that are converted at active centers of a catalyst, *e.g.*, furfuryl alcohol on zeolite crystals.[22] The converted product is fluorescent and all conversions are measured as single-molecule events, localized, and finally summed up to a reactivity map of the catalyst. BALM was used for super-resolution imaging of DNA, exploiting reversible intercalation of YOYO-1 into double stranded DNA.[24] A single intercalation event can be detected with the additional advantage that the quantum yield of YOYO-1 increases by almost 3 orders of magnitude when bound to DNA. Each of these methods can resolve high label densities while being label-free, easy to apply, and without the need for a special buffer environment. However, care has to be taken to minimize nonspecific binding or spontaneous activation of probes especially when used at higher concentrations.

6 Photoswitches without single-molecule localization

An alternative super-resolution method that does not rely on single-molecule localization but still on stochastic blinking or switching of fluorophores is SOFI (super-resolution optical fluctuation imaging), which is based on the analysis of temporal fluorescence fluctuations using higher order statistics.[92] Background-free 3D super-resolution imaging with twofold increase in resolution has been demonstrated.[92] Similar to localization microscopy experiments, an image stack of blinking molecules is recorded and analyzed. When using blinking fluorophores for SOFI, the average dwell time of the nonfluorescent state can be short-lived and high emitter densities can be handled. Therefore, fluorescence intermittencies of semiconductor nanocrystals[92] as well as PS-dyes with a low k_{off}/k_{on} ratio can be used.[93] From the viewpoint of a microscopist, SOFI and localization microscopy together provide a fascinating opportunity: for high k_{off}/k_{on}, isolated emitters can be easily localized and used for localization microscopy. With decreasing k_{off}/k_{on} the emitter density can be insufficient for single-molecule localization algorithms but ideally suited for SOFI.

Nanometer scale measurements are widely performed by fluorescence resonance energy transfer (FRET) experiments. FRET at the single-molecule level is a powerful technique to investigate bimolecular structure and dynamics in the nanometer range.[94] Within a biomolecule, the fluorescence of a FRET unit, *i.e.*, a donor and acceptor fluorophore, is monitored and structural changes can be measured as a change in the FRET efficiency. In complex FRET systems with three or more spectrally different fluorophores, data analysis becomes cumbersome. Here, reversible photoswitchable fluorophores can improve the situation. The method was termed switchable FRET and allows measuring multiple distances within a single biomolecule.[95] Switchable FRET uses two or more spectrally identical photoswitchable acceptor molecules (*e.g.*, Cy5) in combination with a single donor fluorophore. Using alternating laser excitation, switching of the acceptors is induced and fluorescence of the FRET unit is recorded. Because the measured FRET signal depends on variations in donor/acceptor distance, it is crucial which acceptor resides in the *on* state and multiple distances can be measured by analyzing fluorescence time traces from the donor and acceptor detection channel.[95]

Outlook

Without any doubt, photoswitches are key elements of fluorescence imaging with nanometer optical resolution. As an explicit single-molecule technique, localization microscopy helps us to understand fundamental cellular processes. Cellular proteins can be quantified by relating the amount of switching cycles to the absolute molecule number. It is therefore easily comprehensible why scientists are keen on developing efficient photoswitchable FPs and elaborate on chemical cocktails to control the emission pattern of organic dyes. While the development of new photoswitchable FPs is a matter of discovery, mutagenesis and efficient screening, photoswitching of organic dyes is mainly driven by the refined understanding of dye photophysics. Notably, the old design principles of laser dyes have experienced a renaissance. Driven by the upcoming field of single-molecule fluorescence spectroscopy in the 90s of the last century, the photon yield and photostability have been increased first, followed by the development of strategies to minimize fluorescence intermittencies (blinking). A decade later fluorescent dyes that were discarded formerly because of their long-lived dark states have now been reinvented for localization microscopy. Since then, scientists have accepted the challenge of optimizing the photoswitching performance of organic dyes to meet the requirements of various localization microscopy applications.

Acknowledgements

We gratefully acknowledge funding by the Deutsche Forschungsgemeinschaft (DFG; grant SA 829/8-1) and the Bundesministerium für Bildung und Forschung (BMBF; grants 13N11019 and 13N12507). We thank Hannes Neuweiler, Sören Doose and Sven Proppert for critically reading the manuscript and all lab members for their input.

References

1 B. N. G. Giepmans, S. R. Adams, M. H. Ellisman and R. Y. Tsien, *Science*, 2006, **312**, 217–224.
2 M. Irie, *Chem. Rev.*, 2000, **100**, 1685–1716.
3 G. H. Patterson and J. Lippincott-Schwartz, *Science*, 2002, **297**, 1873–1877.
4 M. Irie, T. Fukaminato, T. Sasaki, N. Tamai and T. Kawai, *Nature*, 2002, **420**, 759–760.
5 J. Wiedenmann, S. Ivanchenko, F. Oswald, F. Schmitt, C. Rocker, A. Salih, K. D. Spindler and G. U. Nienhaus, *Proc. Natl. Acad. Sci. U. S. A.*, 2004, **101**, 15905–15910.
6 R. Ando, H. Mizuno and A. Miyawaki, *Science*, 2004, **306**, 1370–1373.
7 M. Heilemann, E. Margeat, R. Kasper, M. Sauer and P. Tinnefeld, *J. Am. Chem. Soc.*, 2005, **127**, 3801–3806.
8 M. Bates, T. R. Blosser and X. W. Zhuang, *Phys. Rev. Lett.*, 2005, **94**, 1749–1753.
9 R. M. Dickson, A. B. Cubitt, R. Y. Tsien and W. E. Moerner, *Nature*, 1997, **388**, 355–358.
10 W. E. Moerner and M. Orrit, *Science*, 1999, **283**, 1670–1676.
11 T. Schmidt, G. J. Schutz, W. Baumgartner, H. J. Gruber and H. Schindler, *Proc. Natl. Acad. Sci. U. S. A.*, 1996, **93**, 2926–2929.
12 R. E. Thompson, D. R. Larson and W. W. Webb, *Biophys. J.*, 2002, **82**, 2775–2783.
13 A. Yildiz, J. N. Forkey, S. A. McKinney, T. Ha, Y. E. Goldman and P. R. Selvin, *Science*, 2003, **300**, 2061–2065.
14 K. Lidke, B. Rieger, T. Jovin and R. Heintzmann, *Opt. Express*, 2005, **13**, 7052–7062.
15 E. Betzig, G. H. Patterson, R. Sougrat, O. W. Lindwasser, S. Olenych, J. S. Bonifacino, M. W. Davidson, J. Lippincott-Schwartz and H. F. Hess, *Science*, 2006, **313**, 1642–1645.
16 M. J. Rust, M. Bates and X. W. Zhuang, *Nat. Methods*, 2006, **3**, 793–795.
17 S. T. Hess, T. P. Girirajan and M. D. Mason, *Biophys. J.*, 2006, **91**, 4258–4272.
18 M. Heilemann, S. van de Linde, M. Schuttpelz, R. Kasper, B. Seefeldt, A. Mukherjee, P. Tinnefeld and M. Sauer, *Angew. Chem., Int. Ed.*, 2008, **47**, 6172–6176.
19 C. Steinhauer, C. Forthmann, J. Vogelsang and P. Tinnefeld, *J. Am. Chem. Soc.*, 2008, **130**, 16840–16841.
20 J. Fölling, M. Bossi, H. Bock, R. Medda, C. A. Wurm, B. Hein, S. Jakobs, C. Eggeling and S. W. Hell, *Nat. Methods*, 2008, **5**, 943–945.
21 A. Sharonov and R. M. Hochstrasser, *Proc. Natl. Acad. Sci. U. S. A.*, 2006, **103**, 18911–18916.
22 M. B. Roeffaers, G. De Cremer, J. Libeert, R. Ameloot, P. Dedecker, A. J. Bons, M. Buckins, J. A. Martens, B. F. Sels, D. E. De Vos and J. Hofkens, *Angew. Chem., Int. Ed.*, 2009, **48**, 9285–9289.
23 G. Giannone, E. Hosy, F. Levet, A. Constals, K. Schulze, A. I. Sobolevsky, M. P. Rosconi, E. Gouaux, R. Tampe, D. Choquet and L. Cognet, *Biophys. J.*, 2010, **99**, 1303–1310.
24 I. Schoen, J. Ries, E. Klotzsch, H. Ewers and V. Vogel, *Nano Lett.*, 2011, **11**, 4008–4011.
25 S. W. Hell, *Nat. Methods*, 2009, **6**, 24–32.
26 G. Patterson, M. Davidson, S. Manley and J. Lippincott-Schwartz, *Annu. Rev. Phys. Chem.*, 2010, **61**, 345–367.
27 J. Vogelsang, C. Steinhauer, C. Forthmann, I. H. Stein, B. Person-Skegro, T. Cordes and P. Tinnefeld, *ChemPhysChem*, 2010, **11**, 2475–2490.
28 B. Huang, H. Babcock and X. Zhuang, *Cell*, 2010, **143**, 1047–1058.
29 S. van de Linde, M. Heilemann and M. Sauer, *Annu. Rev. Phys. Chem.*, 2012, **63**, 519–540.
30 M. G. Gustafsson, *J. Microsc.*, 2000, **198**, 82–87.
31 S. W. Hell and J. Wichmann, *Opt. Lett.*, 1994, **19**, 780–782.
32 K. A. Connors, *Chemical kinetics: The Study of Reaction Rates in Solution*, VCH, New York, 1990.
33 M. Bodenstein, *Z. Phys. Chem.*, 1913, **85**, 329–397.
34 M. Bates, B. Huang, G. T. Dempsey and X. W. Zhuang, *Science*, 2007, **317**, 1749–1753.
35 K. I. Mortensen, L. S. Churchman, J. A. Spudich and H. Flyvbjerg, *Nat. Methods*, 2010, **7**, 377–381.
36 M. Tokunaga, N. Imamoto and K. Sakata-Sogawa, *Nat. Methods*, 2008, **5**, 159–161.
37 P. Annibale, M. Scarselli, A. Kodiyan and A. Radenovic, *J. Phys. Chem. Lett.*, 2010, **1**, 1506–1510.
38 S. H. Lee, J. Y. Shin, A. Lee and C. Bustamante, *Proc. Natl. Acad. Sci. U. S. A.*, 2012, **109**, 17436–17441.
39 P. Sengupta, T. Jovanovic-Talisman, D. Skoko, M. Renz, S. L. Veatch and J. Lippincott-Schwartz, *Nat. Methods*, 2011, **8**, 969–975.
40 S. L. Veatch, B. B. Machta, S. A. Shelby, E. N. Chiang, D. A. Holowka and B. A. Baird, *PLoS One*, 2012, **7**, e31457.
41 D. Lando, U. Endesfelder, H. Berger, L. Subramanian, P. Dunne, J. McColl, D. Klenerman, A. Carr, M. Sauer, R. Allshire, M. Heilemann and E. Laue, *Open Biol.*, 2012, **2**, 120078.
42 S. Wolter, U. Endesfelder, S. van de Linde, M. Heilemann and M. Sauer, *Opt. Express*, 2011, **19**, 7020–7033.
43 S. Wolter, M. Schüttpelz, M. Tscherepanow, S. van de Linde, M. Heilemann and M. Sauer, *J. Microsc.*, 2010, **237**, 12–22.
44 C. S. Smith, N. Joseph, B. Rieger and K. A. Lidke, *Nat. Methods*, 2010, **7**, 373–375.
45 A. Kechkar, D. Nair, M. Heilemann, D. Choquet and J.-B. Sibarita, *PLoS One*, 2013, **8**, e62918.
46 S. Wolter, A. Löschberger, T. Holm, S. Aufmkolk, M. C. Dabauvalle, S. van de Linde and M. Sauer, *Nat. Methods*, 2012, **9**, 1040–1041.
47 S. van de Linde, A. Löschberger, T. Klein, M. Heidbreder, S. Wolter, M. Heilemann and M. Sauer, *Nat. Protocols*, 2011, **6**, 991–1009.
48 H. Shroff, C. G. Galbraith, J. A. Galbraith and E. Betzig, *Nat. Methods*, 2008, **5**, 417–423.
49 S. J. Holden, S. Uphoff and A. N. Kapanidis, *Nat. Methods*, 2011, **8**, 279–280.
50 L. Zhu, W. Zhang, D. Elnatan and B. Huang, *Nat. Methods*, 2012, **9**, 721–723.
51 S. W. Englander, D. B. Calhoun and J. J. Englander, *Anal. Biochem.*, 1987, **161**, 300–306.

52 C. E. Aitken, R. A. Marshall and J. D. Puglisi, *Biophys. J.*, 2008, **94**, 1826–1835.
53 M. Swoboda, J. Henig, H. M. Cheng, D. Brugger, D. Haltrich, N. Plumere and M. Schlierf, *ACS Nano*, 2012, **6**, 6364–6369.
54 Y. Harada, K. Sakurada, T. Aoki, D. D. Thomas and T. Yanagida, *J. Mol. Biol.*, 1990, **216**, 49–68.
55 T. Ha and P. Tinnefeld, *Annu. Rev. Phys. Chem.*, 2012, **63**, 595–617.
56 I. Rasnik, S. A. McKinney and T. Ha, *Nat. Methods*, 2006, **3**, 891–893.
57 J. Widengren, A. Chmyrov, C. Eggeling, P. A. Lofdahl and C. A. Seidel, *J. Phys. Chem. A*, 2007, **111**, 429–440.
58 A. Chmyrov, T. Sanden and J. Widengren, *J. Phys. Chem. B*, 2010, **114**, 11282–11291.
59 J. Vogelsang, R. Kasper, C. Steinhauer, B. Person, M. Heilemann, M. Sauer and P. Tinnefeld, *Angew. Chem., Int. Ed.*, 2008, **47**, 5465–5469.
60 T. Kottke, S. van de Linde, M. Sauer, S. Kakorin and M. Heilemann, *J. Phys. Chem. Lett.*, 2010, **1**, 3156–3159.
61 S. van de Linde, I. Krstic, T. Prisner, S. Doose, M. Heilemann and M. Sauer, *Photochem. Photobiol. Sci.*, 2011, **10**, 499–506.
62 D. Baddeley, D. Crossman, S. Rossberger, J. E. Cheyne, J. M. Montgomery, I. D. Jayasinghe, C. Cremer, M. B. Cannell and C. Soeller, *PLoS One*, 2011, **6**, e20645.
63 A. Lampe, V. Haucke, S. J. Sigrist, M. Heilemann and J. Schmoranzer, *Biol. Cell*, 2012, **104**, 229–237.
64 P. Schäfer, S. van de Linde, J. Lehmann, M. Sauer and S. Doose, *Anal. Chem.*, 2013, **85**, 3393–3400.
65 M. Heilemann, S. van de Linde, A. Mukherjee and M. Sauer, *Angew. Chem., Int. Ed.*, 2009, **48**, 6903–6908.
66 G. T. Dempsey, J. C. Vaughan, K. H. Chen, M. Bates and X. Zhuang, *Nat. Methods*, 2011, **8**, 1027–1036.
67 J. C. Vaughan, G. T. Dempsey, E. Sun and X. W. Zhuang, *J. Am. Chem. Soc.*, 2013, **135**, 1197–1200.
68 J. Vogelsang, T. Cordes, C. Forthmann, C. Steinhauer and P. Tinnefeld, *Proc. Natl. Acad. Sci. U. S. A.*, 2009, **106**, 8107–8112.
69 G. T. Dempsey, M. Bates, W. E. Kowtoniuk, D. R. Liu, R. Y. Tsien and X. Zhuang, *J. Am. Chem. Soc.*, 2009, **131**, 18192–18193.
70 R. Wombacher, M. Heidbreder, S. van de Linde, M. P. Sheetz, M. Heilemann, V. W. Cornish and M. Sauer, *Nat. Methods*, 2010, **7**, 717–719.
71 S. A. Jones, S. H. Shim, J. He and X. Zhuang, *Nat. Methods*, 2011, **8**, 499–505.
72 K. Kundu, S. F. Knight, N. Willett, S. Lee, W. R. Taylor and N. Murthy, *Angew. Chem., Int. Ed.*, 2009, **48**, 299–303.
73 J. C. Vaughan, S. Jia and X. Zhuang, *Nat. Methods*, 2012, **9**, 1181–1184.
74 S. J. Lord, N. R. Conley, H. L. Lee, R. Samuel, N. Liu, R. J. Twieg and W. E. Moerner, *J. Am. Chem. Soc.*, 2008, **130**, 9204–9205.
75 J. Fölling, V. Belov, R. Kunetsky, R. Medda, A. Schonle, A. Egner, C. Eggeling, M. Bossi and S. W. Hell, *Angew. Chem., Int. Ed.*, 2007, **46**, 6266–6270.
76 J. B. Grimm, A. J. Sung, W. R. Legant, P. Hulamm, S. M. Matlosz, E. Betzig and L. D. Lavis, *ACS Chem. Biol.*, 2013, **8**, 1303–1310.
77 K. H. Knauer and R. Gleiter, *Angew. Chem., Int. Ed. Engl.*, 1977, **16**, 113.
78 N. C. Shaner, G. H. Patterson and M. W. Davidson, *J. Cell Sci.*, 2007, **120**, 4247–4260.
79 D. M. Chudakov, M. V. Matz, S. Lukyanov and K. A. Lukyanov, *Physiol. Rev.*, 2010, **90**, 1103–1163.
80 H. Mizuno, T. K. Mal, K. I. Tong, R. Ando, T. Furuta, M. Ikura and A. Miyawaki, *Mol. Cell*, 2003, **12**, 1051–1058.
81 K. Nienhaus, G. U. Nienhaus, J. Wiedenmann and H. Nar, *Proc. Natl. Acad. Sci. U. S. A.*, 2005, **102**, 9156–9159.
82 R. Ando, H. Hama, M. Yamamoto-Hino, H. Mizuno and A. Miyawaki, *Proc. Natl. Acad. Sci. U. S. A.*, 2002, **99**, 12651–12656.
83 P. Dedecker, F. C. De Schryver and J. Hofkens, *J. Am. Chem. Soc.*, 2013, **135**, 2387–2402.
84 U. Endesfelder, S. Malkusch, B. Flottmann, J. Mondry, P. Liguzinski, P. J. Verveer and M. Heilemann, *Molecules*, 2011, **16**, 3106–3118.
85 S. A. McKinney, C. S. Murphy, K. L. Hazelwood, M. W. Davidson and L. L. Looger, *Nat. Methods*, 2009, **6**, 131–133.
86 N. G. Gurskaya, V. V. Verkhusha, A. S. Shcheglov, D. B. Staroverov, T. V. Chepurnykh, A. F. Fradkov, S. Lukyanov and K. A. Lukyanov, *Nat. Biotechnol.*, 2006, **24**, 461–465.
87 F. V. Subach, G. H. Patterson, S. Manley, J. M. Gillette, J. Lippincott-Schwartz and V. V. Verkhusha, *Nat. Methods*, 2009, **6**, 153–159.
88 V. Adam, M. Lelimousin, S. Boehme, G. Desfonds, K. Nienhaus, M. J. Field, J. Wiedenmann, S. McSweeney, G. U. Nienhaus and D. Bourgeois, *Proc. Natl. Acad. Sci. U. S. A.*, 2008, **105**, 18343–18348.
89 T. Grotjohann, I. Testa, M. Leutenegger, H. Bock, N. T. Urban, F. Lavoie-Cardinal, K. I. Willig, C. Eggeling, S. Jakobs and S. W. Hell, *Nature*, 2011, **478**, 204–208.
90 M. Sauer, *Proc. Natl. Acad. Sci. U. S. A.*, 2005, **102**, 9433–9434.
91 T. Brakemann, A. C. Stiel, G. Weber, M. Andresen, I. Testa, T. Grotjohann, M. Leutenegger, U. Plessmann, H. Urlaub, C. Eggeling, M. C. Wahl, S. W. Hell and S. Jakobs, *Nat. Biotechnol.*, 2011, **29**, 942–947.
92 T. Dertinger, R. Colyer, G. Iyer, S. Weiss and J. Enderlein, *Proc. Natl. Acad. Sci. U. S. A.*, 2009, **106**, 22287–22292.
93 T. Dertinger, M. Heilemann, R. Vogel, M. Sauer and S. Weiss, *Angew. Chem., Int. Ed.*, 2010, **49**, 9441–9443.
94 S. Weiss, *Science*, 1999, **283**, 1676–1683.
95 S. Uphoff, S. J. Holden, L. Le Reste, J. Periz, S. van de Linde, M. Heilemann and A. N. Kapanidis, *Nat. Methods*, 2010, **7**, 831–836.

